RevMexAA (Serie de Conferencias), **30**, 64–71 (2007)

WIND-BLOWN BUBBLES AND HII REGIONS AROUND MASSIVE STARS

S. J. Arthur[1]

RESUMEN

La evolución de las estrellas muy masivas está dominada por su pérdida de masa, aunque las tasas de pérdida de masa no se conocen con mucha precisión, particularmente una vez que la estrella sale de la secuencia principal. Los estudios de las nebulosas de anillo y de las cascarones de HI que rodean a muchas estrellas Wolf-Rayet (WR) y variables azules luminosas (LBV) proporcionan algo de información acerca de la historia de la pérdida de masa en las etapas previas. Durante la secuencia principal y la fase WR los vientos estelares hipersónicos forman burbujas en el medio circunestelar e interestelar. Estas dos fases están separadas por una etapa en donde la estrella pierde masa a una tasa muy alta pero a baja velocidad. Por lo tanto, el ambiente presupernova es determinado por la estrella progenitora misma, aún hasta distancias de algunas decenas de parsecs de la estrella. En este artículo, se describen las diferentes etapas en la evolución del medio circunestelar alrededar de una estrella de masa 40 $M_\odot$ mediante simulaciones numéricas.

ABSTRACT

Mass loss dominates the evolution of very massive stars, although the mass loss rates are not known exactly, particularly once the star has left the main sequence. Studies of the ring nebulae and HI shells that surround many Wolf-Rayet (WR) and luminous blue variable (LBV) stars provide some information on the previous mass-loss history. During the main sequence and WR stages, the highly supersonic stellar winds blow bubbles in the interstellar and circumstellar medium. These two stages are separated by phases where the star loses mass with a very high mass-loss rate but at low velocity. The presupernova environment is thus determined by the progenitor itself out to distances of some tens of parsecs from the star. In this article, numerical models are used to illustrate the different stages in the evolution of the circumstellar medium around a 40 $M_\odot$ star.

Key Words: **H II REGIONS — STARS: MASS LOSS**

1. INTRODUCTION

Mass-loss dominates the evolution of very massive stars. Although we can determine directly, with difficulty, the current mass-loss rate and stellar wind terminal velocity, the previous mass-loss history must be inferred from studies of the ring nebulae and HI shells surrounding evolved stars. Massive stars dominate their environment through their photoionizing radiation and stellar winds. Indeed, the energy input into the interstellar and circumstellar medium by winds and ionizing photons can be greater than that of the final supernova explosion, and occurs over a longer timescale.

The currently accepted evolutionary scenario for massive stars is essentially O star to Red Supergiant (RSG) to Wolf-Rayet (WR) star to supernova, for stars more massive than $25M_\odot$ on the main sequence, and O star to RSG to supernova for stars initially below 25 $M_\odot$. The most massive stars will undergo a luminous blue variable (LBV) stage of enhanced, episodic mass loss. Thus, the presupernova circumstellar medium can be very different depending on the initial mass of the progenitor star. For stars that end their lives as red supergiants, the immediate circumstellar medium will be dense and neutral. For stars that have a Wolf-Rayet phase, the circumstellar medium will be dominated by the hypersonic stellar wind and the low-density, hot, shocked bubble it creates.

In this paper, we show, through numerical simulations, how the circumstellar environment of massive stars is shaped by their ionizing photons and strong stellar winds throughout their lives.

2. EARLY EVOLUTION: EMBEDDED H II REGIONS

Massive stars are born in dense molecular clouds and immediately begin to affect their environment through their ionizing photon luminosity. The densities in these regions are very high and the resulting H II regions are very small (< 0.4 pc for compact H II regions and < 0.1 pc for ultracompact H II regions). The observed large numbers of such small ionized regions compared to the estimated formation rate and

[1]Centro de Radioastronomía y Astrofísica, Universidad Nacional Autónoma de México, Apdo. Postal 3–72, 58090 Morelia, Michoacán, México (j.arthur@astrosmo.unam.mx).

lifetimes of massive stars, suggests that some mechanism is responsible for confining these H II regions, or inhibiting their expansion, for up to 10^5 yrs (Wood & Churchwell 1989; Kurtz et al. 1994). This stage, then, represents about 10% of the lifetime of massive stars.

The high extinction in these star-forming regions means that these small, young, ultracompact H II regions are usually only visible at radio and infrarred frequencies. Radio surveys have shown that up to 30% of ultracompact and compact H II regions have a cometary form (Kurtz et al. 1994; Walsh et al. 1998). This suggests that the photoionized gas is expanding off-center in a stratified density distribution, or is moving through its environment. H II regions in density gradients produce champagne flows or blister H II regions, such as those modeled by Tenorio-Tagle and collaborators (Tenorio-Tagle 1979; Bodenheimer et al. 1979). Moving star, or bowshock, models were calculated by Mac Low et al. (1991); van Buren & Mac Low (1992). More recently, numerical simulations of H II regions in density gradients, with and without stellar motion, have been compared in detail with observations by Arthur & Hoare (2006). This latter work shows that it is important to include the stellar wind of the ionizing star in the simulations in order to reproduce the observed radio morphology and infrarred spectra of some well-observed sources. The effect of including the stellar wind in the calculations is shown in Figure 1, where it can be seen that the H II region becomes confined to a roughly hemispherical shell around the hot, shocked wind bubble. Within this shell, a champagne-type flow develops, so although the morphology of the H II region resembles that of a bow-shock model, the kinematics are closer to a champagne flow, which is what has been observed in some well-documented cases (Gaume et al. 1994; Lumsden & Hoare 1999; Zhu et al. 2005).

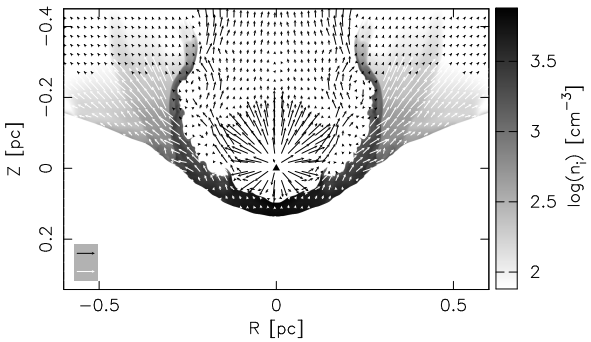

Fig. 1. Logarithm of ionized density (greyscale) and velocity field for a cut through the rz plane of a two-dimensional numerical simulation of an H II region in an exponential plane-stratified density gradient ($n = n_0 \exp(z/H)$ with $n_0 = 8000$ cm^{-3}, scale height $H = 0.2$ pc) with a stellar wind (wind parameters: $\dot{M}_w = 10^{-6}\ M_\odot$ yr^{-1}, $V_w = 2000$ km s^{-1}) after 20,000 yrs of evolution. The velocity field is represented by a split scale: the black arrows show the highest velocity gas $v > 30$ km s^{-1} (generally representing stellar wind gas), while the white arrows are scaled to the lower velocity gas $v \leq 30$ km s^{-1} (present in the photoevaporated flow). The grayscale shows the densest ionized gas in black with a dynamic range of 2 orders of magnitude. Neutral gas, or very low density ionized gas (i.e., stellar wind) appears white.

3. MAIN-SEQUENCE STAGE

As the H II region expands and photoevaporates the maternal molecular cloud, it becomes visible at optical wavelengths. Spectacular images of ionized nebulae such as the Orion Nebula (M82), Trifid Nebula (M20) and the Lagoon Nebula (M8) show the environment of massive stars in this stage of their evolution. The irregular shapes and filaments in these ionized nebulae bear little resemblance to the textbook classical, spherical H II regions. They can be explained simply due to evolution of an H II region in an inhomogeneous medium, such as that produced by turbulence (Mellema et al. 2006), although it is likely that instabilities in the ionization front also play a rôle (García-Segura & Franco 1996; Williams 1999). The evolution of an H II region in a turbulent, clumpy medium is shown in Figure 2. No stellar wind is included in this simulation, but the results show a striking resemblance to observations of real H II regions (and see also Mellema et al. 2006).

A stellar wind appears not to be "necessary" to model the appearance of an H II region in the main sequence stage. Indeed, stellar wind bubbles around main sequence stars are notoriously difficult to detect due to their faintness but there is kinematic evidence of their existence (Nazé et al. 2001). Theory predicts that the initial H II region will become trapped in the shell of dense material that has been swept up by the outer stellar wind shock (Dyson & Williams 1997). The expansion of the ionized gas is then driven by the hot, shocked stellar wind bubble. The H II region establishes itself in the swept-up wind shell and sends an isothermal shock ahead into the neutral gas. So, near the end of the main-sequence stage, the wind bubble consists of a large volume of hot, very low density ionized gas surrounded by a moderately dense photoionized shell at 10^4 K, and outside of this a thick, dense neutral shell expanding at < 10 km s^{-1}, as shown in Fig-

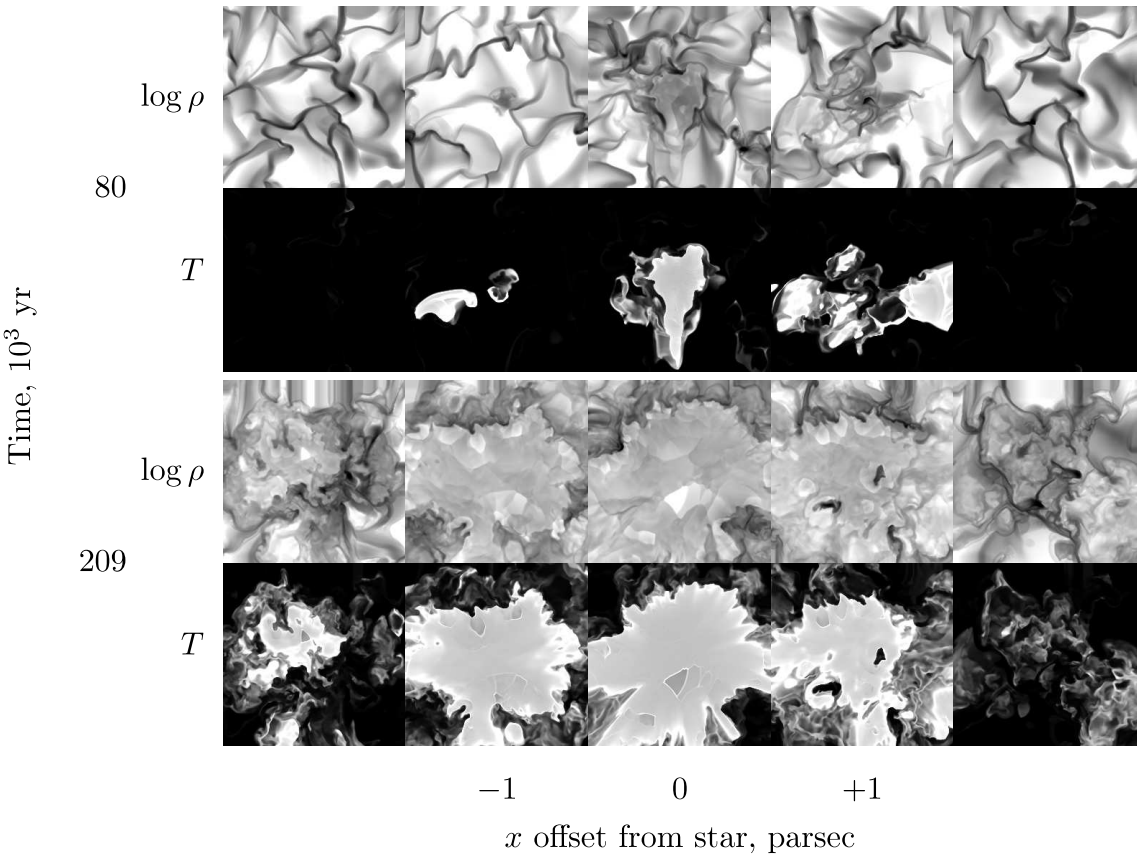

Fig. 2. Dynamical evolution of an H II region in a turbulent, clumpy medium (calculation similar to, but higher resolution than, Mellema et al. 2006). Density and temperature are shown for two different evolutionary times, 80,000 yrs and 209,000 yrs, and five different yz slices through the (4 parsec)^3 computational box (offsets from the ionizing star shown on the bottom axis). The density is shown on a negative logarithmic scale between 10 (white) and 10^5 cm^{-3} (black), while temperature is shown on a positive linear scale between 0 (black) and 10^4 K (white).

ure 3. From this figure it can be seen that the entire wind-bubble structure is at uniform pressure and is expanding slowly into the interstellar medium.

4. POST-MAIN-SEQUENCE EVOLUTION

Classical wind-blown bubble theory (e.g., Dyson & de Vries 1972; Weaver et al. 1977) ceases to be applicable once a star leaves the main sequence. Any subsequent mass loss will occur within the main-sequence stellar wind bubble. A RSG or LBV wind results in a r^{-2} density gradient in the immediate circumstellar medium and it is into this environment that the strong, fast, WR wind expands. An analytical treatment of this scenario was developed by García-Segura & Mac Low (1995a).

Hydrodynamic and radiation-hydrodynamic numerical studies of the evolution of the wind-blown bubbles around stars of initial masses 60 $M_\odot$ and 35 $M_\odot$ have been carried out by García-Segura et al. (1996a,b) and Freyer et al. (2003, 2006). The numerical simulations predict short-lived, observable nebulae during the LBV or RSG stage and during the onset of the WR stage. Instabilities are formed in the dense shells swept-up by the different stellar wind stages, and these are consistent with clumps observed in ring nebulae around some Wolf-Rayet stars. The velocity of the LBV or RSG wind is found to play a key role in the detailed structure of the ring nebulae formed during this process.

A striking example of the interaction between a WR wind and a RSG shell is given by the optical WR ring nebula RCW 58. This nebula consists of clumps and filaments extending radially outward from the central WN8 star, seen in Hα, with more diffuse [O III] emission extending beyond (Chu 1982; Gruendl et al. 2000). The nebula is enriched in He and N, confirming that the material has been ejected from the star, probably during a red supergiant stage.

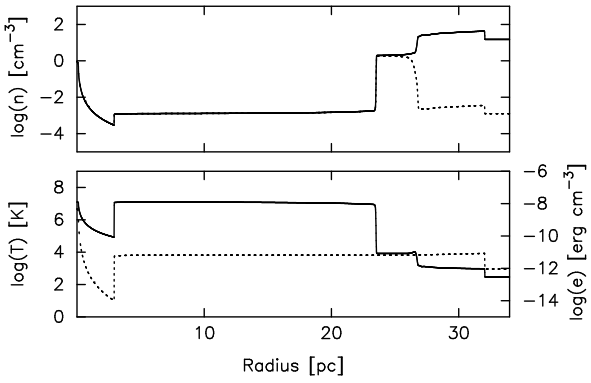

Fig. 3. Radial density and temperature structure of a stellar wind bubble around a $40M_\odot$ star near the end of the main sequence stage (4×10^6 years). Top panel: total number density (solid line) and ionized number density (dotted line). Bottom panel: temperature (solid line) and internal energy ($e = p/[\gamma-1]$ — dotted line). Stellar parameters $\dot{M}_w = 9.1\times10^{-7} M_\odot$ yr $^{-1}$, $V_w = 890$ km s^{-1}, and $S_* = 6.34 \times 10^{47}$ s^{-1}, ambient density $n = 12$ cm^{-3} and temperature $T = 200$ K (adapted from van Marle et al. 2005).

The reality of this high mass-loss rate, low velocity post-main-sequence mass loss is much messier than described here. The mass loss can be asymmetric and episodic, with complex velocity structure, even if the star does not undergo an LBV stage (see Humphreys 2007). However, to simplify the discussion, we assume that the mass loss in this stage is homogeneous, isotropic and uniform with time.

A 40 $M_\odot$ star will have a RSG stage, during which its ionizing photon luminosity falls to a negligible value, and the stellar wind velocity drops to 15 km s^{-1} while the mass-loss rate increases to 8.3×10^{-5} $M_\odot$ yr^{-1} (van Marle et al. 2005). This phase is short lived, $< 2 \times 10^5$ years. As the slow, dense, neutral RSG wind expands into the main-sequence wind bubble, a thin, dense shell of shocked RSG material forms ahead of the freely expanding RSG wind. The drop in ionizing photon rate leads to recombination of the H II region in the outer shell, although the hot bubble remains ionized due to the long recombination times in this very low-density gas.

At the end of the RSG phase, the mass-loss rate remains high while the stellar wind velocity increases substantially and the ionizing photon rate returns almost to the level it was in the main sequence stage. The transition between the slow, dense RSG wind and the fast WR wind will involve a period of wind acceleration into the r^{-2} density distribution left by the RSG wind, and this situation is inherently Rayleigh-Taylor unstable. Clumps and filaments of dense, neutral material form in the interaction region as the WR wind drives a shock into the RSG shell (e.g., García-Segura et al. 1996b; Freyer et al. 2003). These clumps lag behind the main swept-up WR shell but the shell itself does not break up, since the instabilities stop growing once the acceleration stage finishes. The clumps and filaments are photo- and hydrodynamically ablated and the evaporating material is shocked and heated to X-ray emitting temperatures as it mixes into the hot shocked WR wind gas.

In Figure 4 we show the temperature and ionized density structure of a two-dimensional simulation of the interaction between the WR wind and the RSG wind of the 40 $M_\odot$ star described above. During the RSG phase, 16.5 $M_\odot$ of stellar material were expelled in the slow, dense wind and this is swept up into a shell by the fast WR wind. The swept-up RSG material dominates the density map and becomes ionized by the central star as it expands outwards and the opacity drops. Rayleigh-Taylor instabilities have caused fingers of dense RSG material to protrude into the low-density WR wind, and Kelvin-Helmholtz instabilities have shaped these structures into filaments and clumps. The clumps are very dense and some have neutral cores. They are reasonably long lived due to their enhanced cooling rates and so are sources of mass loading of the WR wind (Hartquist et al. 1986; Arthur et al. 1993, 1996).

5. X-RAY EMISSION FROM WOLF-RAYET NEBULAE

Of the $\sim$ 150 known Wolf-Rayet stars in the Galaxy, only ~ 10 of these have wind-blown bubbles around them, where a wind-blown bubble is characterized by a sharp rim and a short dynamical age (Chu 1981; Lozinskaya 1982).[2] To date, four of these objects have been observed with X-ray satellites but only two of them, NGC 6888 and S 308, have been detected in diffuse X-rays.

The observations of NGC 6888 and S 308 reveal very soft X-ray spectra, with the main component of the spectra corresponding to X-ray emitting gas

[2]These objects are: S 308, RCW 58, RCW 104, NGC 2359, NGC 3199, NGC 6888, Anon (MR26), G2.4+1.4, and there is kinematical evidence that the nebulae around WR 116 and WR 133 have expansion velocities consistent with wind-blown bubbles (Esteban & Rosado 1995). Anon(WR 128) and Anon(WR 134) are possibly wind-blown bubbles, too (Gruendl et al. 2000). There are also wind-blown bubbles around two other evolved stars: NGC 6164-5 (around an O6.5fp star), NGC 7635 (around an O6.5III star).

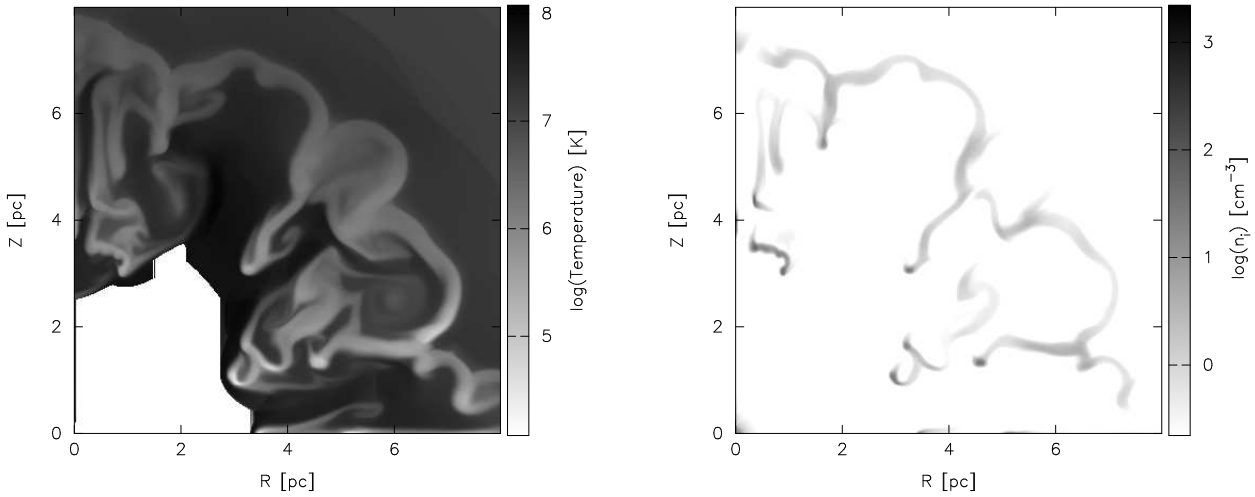

Fig. 4. Interaction of the Wolf-Rayet wind with the dense shell from the red supergiant stage for a $40M_{\odot}$ star. The WR wind parameters are a mass-loss rate of $\dot{M}_w = 4.1 \times 10^{-5}$ $M_{\odot}$ yrs^{-1} and a stellar wind velocity of $V_w = 2160$ km s^{-1}, and the star has an ionizing photon rate of $S_* = 3.86 \times 10^{47}$ s^{-1}. *(a)* Gas temperature and *(b)* ionized number density 24,000 years after the onset of the WR wind. The central white area is the unshocked WR wind, assumed to have a temperature $T \leq 10^4$ K.

temperatures of 1.5×10^6 K and 1.0×10^6 K, respectively (Bochkarev 1988; Wrigge et al. 1994; Wrigge 1999; Chu et al. 2003). The softness of these X-ray spectra suggest a possible explanation for the non-detection of X-rays in the other wind-blown bubbles, namely that extinction plays an important rôle (Y.-H. Chu, priv. comm.). For X-ray emitting gas temperatures in the range 1–5×10^6 K such a large fraction of the emitted flux can be absorbed by the intervening HI column that the fitted temperature depends strongly on the column density of neutral hydrogen (Wrigge et al. 2005).

Another possible explanation for the non-detection of X-rays from WR wind-blown bubbles is that the X-ray emitting stage is relatively short-lived, lasting, say, only 20% of the time the WR wind is interacting with the RSG shell. In Figure 5 we show the variation of total X-ray luminosity with elapsed time in the WR stage during the interaction of the WR wind with the RSG shell for the $40M_{\odot}$ star simulation described above. The total X-ray luminosity of the model is larger in magnitude than either that obtained for NGC 6888 ($\sim 9 \times 10^{34}$ erg s^{-1} from *ASCA* observations, Wrigge et al. 2005), or S 308 ($\sim 1 \times 10^{34}$ erg s^{-1} from *XMM* observations, Chu et al. 2003). The parameters of the simulation have not been tailored to any particular object and the X-ray emission is very sensitive both to the absorbing H I column density and to the amount of mass expelled in the RSG phase and swept up by the WR wind (see Wrigge et al. 2005). Figure 5 shows that in the simulation, the X-rays become slightly harder with time, due to expansion of the X-ray emitting structures and the reduction in their density and corresponding cooling rates. The absorbing H I column obviously has an impact on the observed X-ray luminosity since most of the emission comes from the energy range $E < 1$ keV.

In this work, the X-rays are calculated assuming collisional ionization equilibrium, taking into account both line and continuum emission processes and assuming solar abundances. Solar abundances are obviously not entirely appropriate for this situation since the evolving star will enhance the metallicity of its surface layers, which are then lost to the stellar wind, as time proceeds. However, without including a detailed description of the stellar evolution in our models, we cannot follow the changing abundances in the circumstellar medium (see Pérez-Rendón 2006). The calculated X-ray spectrum is then corrected for absorption using the procedure described by Wilms et al. (2000), and finally it is folded through the *Chandra* ACIS-SIS instrument response matrices.

The gas responsible for the X-ray emission comes from the interaction of the WR wind with the RSG shell. However, this interaction leads to instabilities in the dense shell, and the formation of Rayleigh-Taylor fingers, then filaments and clumps. These clumps and filaments contain reservoirs of dense neu-

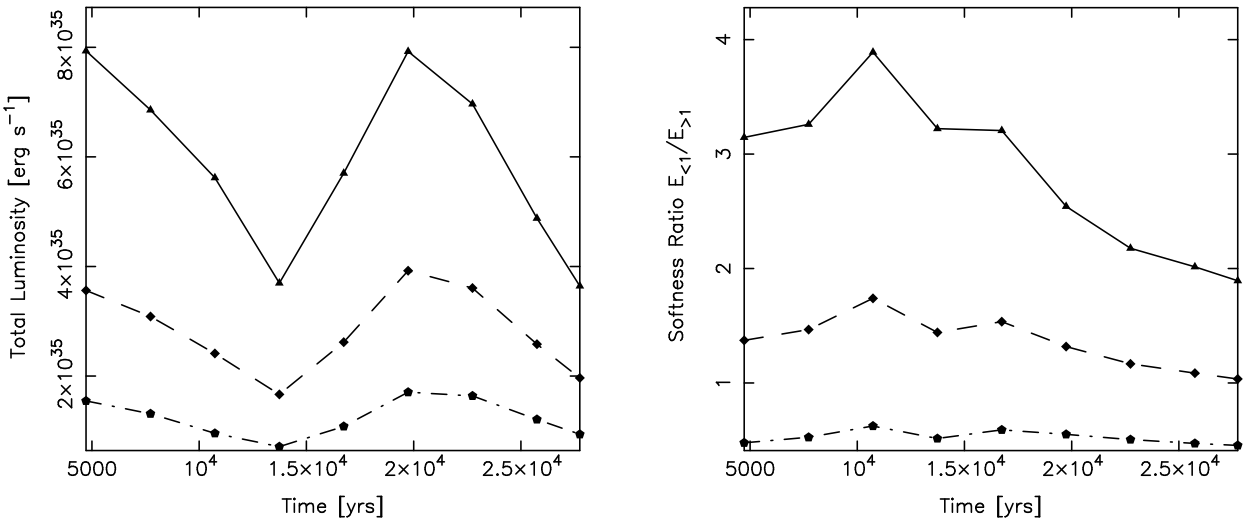

Fig. 5. *(a)* X-ray luminosity against time in the WR stage for the 2D numerical simulation describing the interaction of the WR wind with the RSG shell. *(b)* Ratio of luminosity for the energy band < 1 keV to that of the energy band > 1 keV. The three lines represent different neutral hydrogen column densities: Solid line — $N_H = 2 \times 10^{21}$ cm^{-2}, dashed line — $N_H = 5 \times 10^{21}$ cm^{-2}, dot-dash line — $N_H = 10 \times 10^{21}$ cm^{-2}.

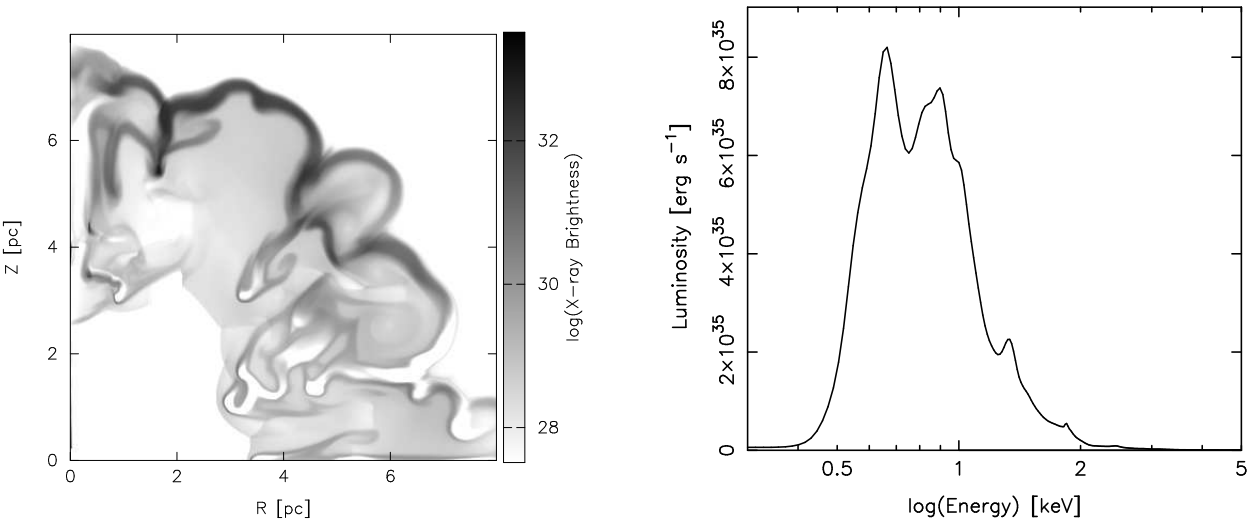

Fig. 6. *(a)* X-ray brightness for a thin wedge of the numerical simulation. *(b)* X-ray spectrum integrated over the whole object for the simulation shown in Figure 4. An absorbing neutral hydrogen column density $N_H = 2.0 \times 10^{21}$ cm^{-2} is assumed.

tral gas, which are photoevaporated by the ionizing photons from the hot star. The dense photoevaporated flow interacts with the fast stellar wind and produces swept-back regions of relatively dense gas at $\sim 10^6$ K. Also, the main shock traveling through the dense shell is a source of X-ray emission. In Figure 6 we show the X-ray brightness of a thin wedge of the 2-D simulation for a time towards the end of the range shown in Figure 5 and an absorbing column density $N_H = 2.0 \times 10^{21}$ cm^{-2}. Also shown in Figure 6 is the corresponding X-ray spectrum for the whole object at the same time. From these figures it can be seen that the X-ray emission comes as much from shocked clumps and filaments as from behind the principal shock. The X-ray spectrum obtained from this simulation is soft, with the peak emission

coming at around 0.5 – 1 keV, although not as soft as that observed for S 308.

In order to explain the amount and softness of the X-rays emitted by wind-blown bubbles it has been argued that nebular material from the RSG shell must be mixed into the X-ray emitting gas, both to increase the density and to enhance the cooling rate (Chu et al. 2003; Wrigge et al. 2005). This mixing could be due to thermal evaporation of the cold shell by the hot bubble or by hydrodynamic ablation of embedded clumps and filaments. Our simulations show that the embedded clumps and filaments are, indeed, important for the X-ray emission, both through the interaction of photoevaporated flows with the shocked stellar wind and through hydrodynamic processes. We have not included thermal conduction in our calculations, and we comment that this additional mass-loading process is not necessary in the present simulation to reproduce the X-ray luminosities reported in the observations.

6. FINAL STAGES

By the end of the WR stage, the circumstellar medium around the star consists of a low-density bubble of hot, shocked WR wind surrounded by the remnants of the main sequence wind bubble, a reionized exterior H II region and neutral shell. This is shown in Figure 7.

Many Wolf-Rayet stars are surrounded by multiple concentric shells of material, observable at infrared or 21 cm radio wavelengths and in about 8% of cases even optically (Marston 1996). The outermost shells can have diameters up to 100 pc and are expanding slowly (generally, $v_{\rm exp} < 10$ km s^{-1} Marston 1996; Cappa et al. 2005). These structures were mainly formed during the main-sequence stage. The innermost shells are often visible in optical narrowband images, and represent material ejected during the RSG or LBV stage photoionized by the WR star. In a few cases, there is evidence for dynamical shaping of a nebula by the WR wind (Chu 1981; Lozinskaya 1982).

It is into this circumstellar medium that the supernova remnant will expand. Just as each subsequent stellar evolutionary stage reveals the structure formed around the star by the previous stage, so too do the supernova event and expansion of the supernova remnant help to uncover the structure of the surrounding circumstellar and interstellar medium. Gamma-ray burst afterglows probe the innermost regions of the progenitor wind bubble (Chevalier et al. 2004), and Type II and Type Ib/c supernova narrow spectral absorption features can be attributed to moving shells around the massive star progenitor (Dopita et al. 1984). The first ~ 1000 years of supernova remnant expansion occur within the immediate circumstellar medium of the progenitor and the interaction of the ejecta with the ambient medium, observed across the electromagnetic spectrum, can reveal important clues as to the nature of the progenitor star. In some cases, however, more puzzles are created, such as the Cas A supernova remnant.

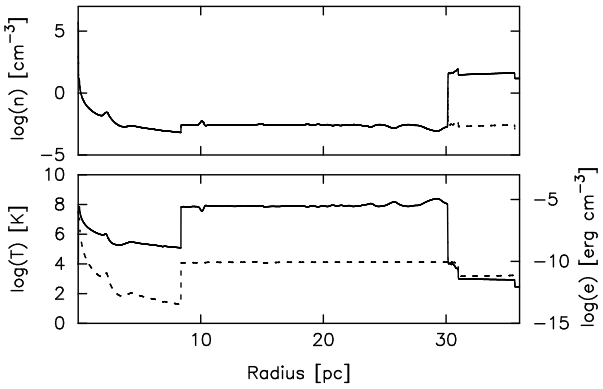

Fig. 7. Radial structure of a stellar wind bubble around a 40 $M_\odot$ star at the end of the Wolf-Rayet phase, i.e. after a total time of $\sim 4.8 \times 10^6$ years. Top panel: total number density (solid line) and ionized number density (dotted line). Bottom panel: temperature (solid line) and internal energy ($e = p/[\gamma - 1]$ — dotted line).

7. CONCLUSIONS

The basic theory of the formation and evolution of wind-blown bubbles and H II regions around massive stars has been well understood for quite some time. However, the classical picture does not withstand a detailed comparison with observations. Instabilities play a fundamental rôle in the formation of structure and the generation of emission features, both at optical and X-ray wavelengths. The finer details of the mass-loss episodes in the RSG and LBV stages are the key to understanding the immediate circumstellar medium at the onset of the WR stage.

REFERENCES

Arthur, S. J., Dyson, J. E., & Hartquist, T. W. 1993, MNRAS, 261, 425
Arthur, S. J., Henney, W. J., & Dyson, J. E. 1996, A&A, 313, 897
Arthur, S. J., & Hoare, M. G. 2006, ApJS, 165, 283
Bochkarev, N. G. 1988, Nature, 332, 518
Bodenheimer, P., Tenorio-Tagle, G., & Yorke, H. W. 1979, ApJ, 233, 85

Cappa, C., Niemela, V. S., Martín, M. C., & McClure-Griffiths, N. M. 2005, A&A, 436, 155
Chevalier, R. A., Li, Z.-Y., & Fransson, C. 2004, ApJ, 606, 369
Chu, Y.-H. 1981, ApJ, 249, 195
_____. Y.-H. 1982, ApJ, 254, 578
Chu, Y.-H., Guerrero, M. A., Gruendl, R. A., García-Segura, G., & Wendker, H. J. 2003, ApJ, 599, 1189
Dopita, M. A., Cohen, M., Schwartz, R. D., & Evans, R. 1984, ApJ, 287, L69
Dyson, J. E., & de Vries, J. 1972, A&A, 20, 223
Dyson, J. E., & Williams, D. A. 1997, The Physics of the Interstellar Medium (2nd edition; Bristol: IOP)
Esteban, C., & Rosado, M. 1995, A&A, 304, 491
Freyer, T., Hensler, G., & Yorke, H. W. 2003, ApJ, 594, 888
_____. 2006, ApJ, 638, 262
García-Segura, G., & Franco, J. 1996, ApJ, 469, 171
García-Segura, G., & Mac Low, M.-M. 1995a, ApJ, 455, 145
García-Segura, G., Mac Low, M.-M., & Langer, N. 1996a, A&A, 305, 229
García-Segura, G., Langer, N., & Mac Low, M.-M. 1996b, A&A, 316, 133
Gaume, R. A., Fey, A. L., & Claussen, M. J. 1994, ApJ, 432, 648
Gruendl, R. A., Chu, Y.-H., Dunne, B. C., & Points, S. D. 2000, AJ, 120, 2670
Hartquist, T. W., Dyson, J. E., Pettini, M., & Smith, L. J. 1986, MNRAS, 221, 715
Humphreys, R. 2007, RevMexAA (SC), 30, 6
Kurtz, S., Churchwell, E., & Wood, D. O. S. 1994, ApJS, 91, 659
Lozinskaya, T. A. 1982, Ap&SS, 87, 313
Lumsden, S. L., & Hoare, M. G. 1999, MNRAS, 305, 701
Mac Low, M.-M., van Buren, D., Wood, D. O. S., & Churchwell, E. 1991, ApJ, 369, 395
Marston, A. P. 1996, AJ, 112, 2828
Mellema, G., Arthur, S. J., Henney, W. J., Iliev, I. T., & Shapiro, P. R. 2006, ApJ, 647, 397
Nazé, Y., Chu, Y.-H., Points, S. D., Danforth, C. W., Rosado, M., & Chen, C.-H. R. 2001, AJ, 122, 921
Pérez-Rendón, B. 2006, PhD Thesis, UNAM, México
Tenorio-Tagle, G. 1979, A&A, 71, 59
van Buren, D., & Mac Low, M.-M. 1992, ApJ, 394, 534
van Marle, A. J., Langer, N., & García-Segura, G. 2005, A&A, 444, 837
Walsh, A. J., Burton, M. G., Hyland, A. R., & Robinson, G. 1998, MNRAS, 301, 640
Weaver, R., McCray, R., Castor, J., Shapiro, P., & Moore, R. 1977, ApJ, 218, 377
Williams, R. J. R. 1999, MNRAS, 310, 789
Wilms, J., Allen, A., & McCray, R. 2000, ApJ, 542, 914
Wood, D. O. S., & Churchwell, E. 1989, ApJS, 69, 831
Wrigge, M., Wendker, H. J., & Wisotzki, L. 1994, A&A, 286, 219
Wrigge, M. 1999, A&A, 343, 599
Wrigge, M., Chu, Y.-H., Magnier, E. A., & Wendker, H. J. 2005, ApJ, 633, 248
Zhu, Q.-F., Lacy, J. H., Jaffe, D. T., Richter, M. J., & Greathouse, T. K. 2005, ApJ, 631, 381